Viscous flow properties and hydrodynamic diameter of phenothiazine-based redox-active molecules in different supporting salt environments

Yilin Wang (王怡琳)[a,b,c], Aman Preet Kaur[d,e], N. Harsha Attanayake[d,e], Zhou Yu (于洲)[f], Thilini M. Suduwella[d,e], Lei Cheng (程蕾)[f], Susan A. Odom[d,e], and Randy H. Ewoldt[*,a,b,c,g]

[a] *Department of Mechanical Science and Engineering, University of Illinois at Urbana-Champaign, Urbana, IL 61820 USA*
[b] *Beckman Institute for Advanced Science and Technology, University of Illinois at Urbana-Champaign, Urbana, IL 61820 USA*
[c] *Joint Center for Energy Storage Research, Urbana, IL 61820 USA*
[d] *Joint Center for Energy Storage Research, Lexington, KY 40506 USA*
[e] *Department of Chemistry, University of Kentucky, Lexington, KY 40506, USA*
[f] *Materials Science Division and Joint Center for Energy Storage Research, Argonne National Laboratory, Lemont, IL 60439 USA*
[g] *Materials Research Laboratory, University of Illinois at Urbana-Champaign, Urbana, IL 61820 USA*

* **Author to whom correspondence should be addressed**: ewoldt@illinois.edu.

ABSTRACT

We report viscous flow properties of a redox-active organic molecule, *N*-(2-(2-methoxyethoxy)ethyl)phenothiazine (MEEPT), a candidate for non-aqueous redox flow batteries, and two of its radical cation salts. A microfluidic viscometer enabled the use of small sample volumes in determining viscosity as a function of shear rate and concentration in the non-aqueous solvent, acetonitrile, both with and without supporting salts. All solutions tested show Newtonian behavior over shear rates of up to 30,000 s^{-1}, which was rationalized by scaling arguments for the diffusion-based relaxation time of a single MEEPT molecule without aggregation. Neat MEEPT is flowable but with a large viscosity (412 $mPa \times s$ at room temperature), which is approximately 1,000 times larger than that of acetonitrile. MEEPT solutions in acetonitrile have low viscosities; at concentrations up to 0.5 M, the viscosity increases by less than a factor of two. From concentration-dependent viscosity measurements, molecular information was inferred from intrinsic viscosity (hydrodynamic diameter) and the Huggins coefficient (interactions). Model fit credibility was assessed using the Bayesian Information Criterion (BIC). It is found that the MEEPT and its charged cation are "flowable" and do not flocculate at concentrations up to 0.5 M. MEEPT has a hydrodynamic diameter of around 8.5 Å, which is almost insensitive to supporting salt and state of charge. This size is comparable to molecular dimensions of single molecules obtained from optimized structures using density function theory calculations. The results suggest that MEEPT is a promising candidate for redox flow batteries in terms of its viscous flow properties.

1. INTRODUCTION

Non-aqueous redox flow batteries (NAqRFBs) utilizing solutions of redox-active organic molecules (ROMs) are competitive for reliable electrochemical energy storage systems due to their scalable energy capacity, large electrochemical stability windows, and potentially long operating lifetimes.[1–6] In NAqRFBs, charges are stored in ROMs and transported by ionic supporting salts, both dissolved in an organic solvent. From a techno-economic study,[2,7] the concentration of active materials must be larger than 1 M for NAqRFBs to be competitive, with a target concentration of 5 M. Previous research has shown that highly concentrated electrolytes can result in dramatically increased viscosities.[8] The performance of RFBs is heavily dependent on the viscosity of electrolytes, with higher viscosities having a negative influence on key transport properties,[9] such as ionic conductivity[10] and diffusivity.[11,12] Viscosity is also directly related to pumping costs.[13] Bindner *et al.* reported an 8-11% of total power loss from pumping for a vanadium RFB.[14] Understanding the origin of viscosity differences in these complex fluids is therefore of interest in the development of solutions with favorable properties.

Studies evaluating the viscous flow properties of electrolytes for RFBs show that the concentration-dependent viscosities of electrolytes can be affected by ROM size[15,16] and its state of charge,[17,18] solution temperature,[19] inclusion of additives,[20] and ionic strength of supporting salts.[21] Great efforts have been made in predicting electrolyte viscosity, e.g., models based on Eyring's absolute theory,[22] transition-state theory,[23–25] and the Advanced Electrolyte Model (AEM).[9,26] However, no universal method accounts for all factors that affect the viscosity, and experimental calibration is needed for some model parameters. Furthermore, few publications discuss non-Newtonian behavior of ROM electrolytes, which might arise from flow-induced conformation of ROMs[27] and the break-up of interactions between them.[28] Non-Newtonian analysis matters in non-equilibrium molecular dynamics (NEMD) simulations,[29–33] as the NEMD simulation may study flows in the large Weissenberg number (Wi) regime (very high shear rates), where viscosities show non-Newtonian behavior. For instance, Zhang *et al.*[34] used NEMD to calculate shear viscosity of imidazolium-based ionic liquids at shear rates in the range 10^7–10^9 s^{-1}, where shear-thinning was observed. Therefore, to optimize the operating condition of RFBs, experimental viscous flow properties of ROM solutions must be considered.

In this study, the viscous flow properties of *N*-(2-(2-methoxyethoxy)ethyl)phenothiazine (MEEPT) were studied using a microfluidic viscometer (Figure 1(a)). This enables viscosity measurement using small sample volumes and a wide range of shear rates around two orders of magnitude. MEEPT is a ROM that shows promise for meeting grid-scale energy storage requirements, as evidenced by its high current density and long duration cycling.[35] However, its viscosity and other transport properties, such as diffusivity and ionic conductivity, have not been reported. Here we measured the concentration-dependent viscosities of neutral MEEPT, its tetrafluoroborate radical-cation salt (MEEPT-BF_4), and its bis(trifluoromethanesulfonyl)imide salt (MEEPT-TFSI) at different concentrations in acetonitrile (ACN) and in ACN-based electrolytes containing different supporting salts, namely, tetraethylammonium tetrafluoroborate ($TEABF_4$) and lithium bis(trifluoromethanesulfonyl)imide (LiTFSI). For concentration-dependent viscosities, the Einstein,[36] Huggins,[37] and extended Jones-Dole equations[38] were used to fit and understand the measured viscosities. From fit results, molecular information, such as intrinsic viscosity, hydrodynamic diameter, Huggins coefficient, and the presence of ion interactions can be

determined. The residual sums of squares (RSS) were used and the Bayesian Information Criteria (BIC) of the fits were compared to determine the most credible fit. A simple estimate of the relaxation time scale of MEEPT was used to understand the observed Newtonian behavior of MEEPT solutions.

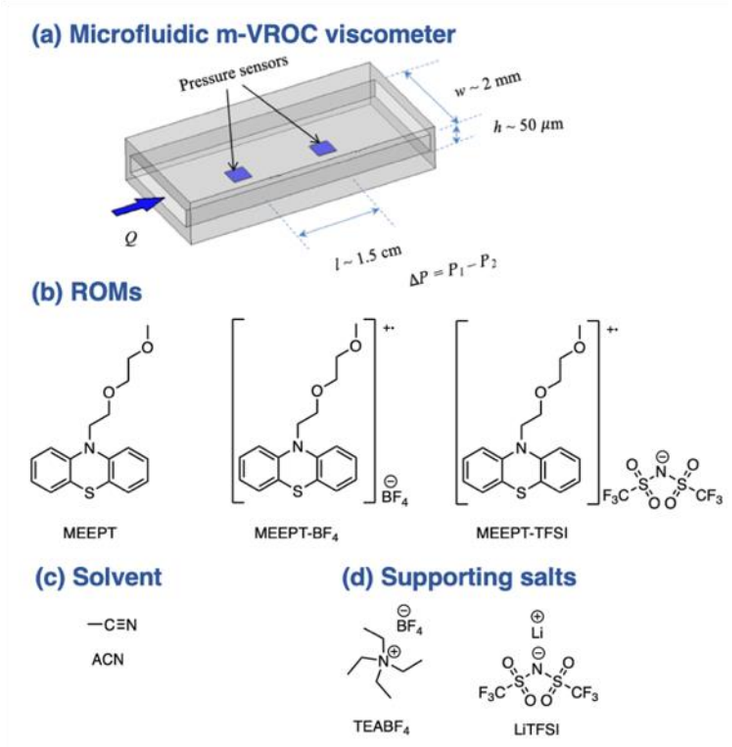

Figure 1. Representation of (a) microfluidic viscometer (image adapted from RheoSense Inc.), (b) ROMs: MEEPT (neutral), MEEPT-BF_4 (charged), and MEEPT-TFSI (charged), (c) solvent: acetonitrile (ACN), and (d) supporting salts: $TEABF_4$ and LiTFSI.

The hydrodynamic diameter of MEEPT remains essentially unchanged with the addition of supporting salts and is comparable to the molecular structure dimensions, which suggests minimal flocculation and small solvation shells for MEEPT in supporting salt environments. The Huggins coefficients are of the same order of magnitude, but larger than that of Brownian hard spheres in shear flow as derived by Batchelor,[39] suggesting that interactions other than hydrodynamic interactions and steric effects contribute to viscous dissipation. Our results ultimately show that (i) both neutral and charged MEEPT are "flowable" ROMs, and their solution viscosities increase with concentration as a result of excluded volume and interactions between ROMs, (ii) addition of supporting salts does not have a dramatic influence on the hydrodynamic diameter of MEEPT, but it does affect the interactions between MEEPT molecules, (iii) the viscosities increase in the charged form of MEEPT, which arises from the volume excluded by corresponding anions, and (iv) there is minimal flocculation within the concentrations and shear rates tested, and the critical shear rate, the rate at which the solution begins to show shear-thinning, is larger than limits experimentally accessed.

2. MATERIALS AND METHODS

A. Materials

The redox-active molecule MEEPT (301.40 g/mol) was obtained from TCI, and its radical cation salts, MEEPT-BF_4[35] and MEEPT-TFSI[40] were synthesized as described in the Supporting Information. Two supporting salts, LiTFSI (Aldrich, 99.95%) and $TEABF_4$ (Aldrich, 99%), were chosen because these are both commonly used in RFBs and they affect the solubility of charged MEEPT differently, as shown in
Table **1**. All ROMs and salts were dissolved in acetonitrile (ACN) to reduce ion associations, as ACN is the most polar organic solvent with a wide electrochemical stability window,[41,42] and therefore, commonly employed in NAqRFBs.

B. Viscometry

The dynamic viscosity of solutions was measured using a microfluidic viscometer m-VROC (RheoSense Inc.). Only microliter sample volumes are required by this viscometer, and free surface effects,[43] evaporation, and contamination can be avoided during the measurement due to internal flow. The measuring chip is made from borosilicate glass containing a rectangular slit flow channel with uniform cross-section, as shown in Figure 1(a).[44] The fluid sample is pushed by a syringe pump at a constant volume flow rate, Q, which is related to the apparent shear rate, $\dot{\gamma}_{\text{app}}$, by[27]

$$\dot{\gamma}_{\text{app}} = \frac{6Q}{wh^2}, \tag{1}$$

where w and h are the width and the height of the channel respectively (2 mm × 50 μm). The actual shear rate at the wall, $\dot{\gamma}$, is related to $\dot{\gamma}_{\text{app}}$ as[27]

$$\dot{\gamma} = \frac{\dot{\gamma}_{\text{app}}}{3}\left[2 + \frac{d\ln\left(\dot{\gamma}_{\text{app}}\right)}{d\ln\left(\tau\right)}\right] = \dot{\gamma}_{\text{app}}\left[\frac{2}{3} + \frac{1}{3}\frac{d\ln\left(Q\right)}{d\ln\left(\Delta p\right)}\right]. \tag{2}$$

For Newtonian fluids and laminar flow, the shear stress, t, is linearly proportional to $\dot{\gamma}_{\text{app}}$, so $\dot{\gamma} = \dot{\gamma}_{\text{app}}$. For non-Newtonian fluids, the shear rate needs to be modified using Eq. (2) to calculate the true viscosity. Four pressure sensors are mounted at the boundary wall in the channel to detect the pressure drop from the inlet to the outlet as a function of position along the channel, and t is calculated from the pressure drop as[27]

$$t = \frac{\Delta p}{L}\frac{wh}{2w + 2h}, \tag{3}$$

where Δp is the measured pressure drop, and L is the channel length over which Δp is measured (15 mm). Two different microchips were used, each with the same dimensions but different pressure measurement ranges, having maximum measurable pressure drops, $\Delta p_{\max}$, of 10,000 and 40,000 Pa respectively, and with a minimum measurable pressure drop of 1% of the maximum. These limits, together with the maximum flow rate, bound the range of measurable viscosity versus shear rate. The dynamic viscosity is defined as[45]

$$\eta \equiv \frac{\tau}{\dot{\gamma}}. \tag{4}$$

Experimental limits constrain the range of $\dot{\gamma}$ available to explore non-Newtonian behavior, which are converted to experimental windows,[43] as shown in the viscosity versus shear rate plots. For each solution, viscosities were measured within a wide shear rate range (5,000-30,000 s^{-1}) for most samples, which varied depending on the viscosity of each solution. This corresponds to a relevant range for RFBs, which can be estimated from conditions in literature. For instance, laboratory-scale RFBs[46,47] may have channel diameters, $2R$, as small as 1-3 mm with flow rate, Q, 10–100 mL/min. From Poiseuille flow of a Newtonian fluid in a circular tube, the wall shear rate is $\dot{\gamma} = \frac{4}{\pi}\frac{Q}{R^3}$, giving an upper-bound estimate of shear rate around 100–20,000 s^{-1}. The temperature was maintained at 25ºC by a Thermocube circulator. For each sample, repeat measurements were done in triplicate with the same solution including separate syringe loading (except when the sample volume was limited for which only one or two were possible), and the uncertainty was calculated as the standard deviation.

Table 1. The solubilities of ROMs in different supporting salt environments and composition of solutions investigated in this study.

ROM	Electrolyte	Solubility (M)	Maximum concentrations tested in this study (M)
MEEPT	ACN	miscible	3.78
	0.5 M $TEABF_4$/ACN	miscible	1.00
	0.5 M LiTFSI/ACN	miscible	1.00
MEEPT-BF_4	ACN	0.55	0.45
	0.5 M $TEABF_4$/ACN	0.45	0.36
	0.5 M LiTFSI/ACN	0.81	0.43
MEEPT-TFSI	ACN	1.54	1.00
	0.5 M $TEABF_4$/ACN	1.11	1.00
	0.5 M LiTFSI/ACN	1.18	1.00

C. Viscosity models

To describe the concentration-dependent viscosity, the equations used are listed here. For solutions containing uncharged particles, Einstein formulated an equation to theoretically calculate the viscosity of dilute molecular solutions of rigid, non-attracting spheres at different concentrations,[36] as

$$\frac{\eta(f)}{\eta_s} = 1 + \frac{5}{2}f + O\left(f^2\right), \tag{5}$$

where $\eta(f)$ and η_s are the viscosities of solution and solvent respectively, and f is the volume fraction of solute particles. For spherical particles, f can be written as

$$f = \frac{4}{3}p\left(\frac{d_H}{2}\right)^3 cN_A, \tag{6}$$

where d_H is the hydrodynamic diameter of an individual particle, c is the concentration (moles per volume), and N_A is Avogadro's constant. Thus, the Einstein equation can be written in terms of concentration as

$$\frac{\eta(c)}{\eta_s} = 1 + [\eta]c + O\left(c^2\right), \tag{7}$$

where $[h]$ is the intrinsic viscosity, which is a function of only d_H, such that

$$[h] = \frac{10}{3}p\left(\frac{d_H}{2}\right)^3 N_A. \tag{8}$$

Experimentally, Huggins expanded this equation to a more concentrated regime, with a higher-order term representing the particle interactions,[37]

$$\frac{\eta(c)}{\eta_s} = 1 + [\eta]c + k_H\left([\eta]c\right)^2 + O\left(c^3\right), \tag{9}$$

which is called the Huggins equation, where k_H is the Huggins coefficient that quantifies the interactions between particles. For Brownian hard spheres with only hydrodynamic interactions and steric effects, Batchelor numerically derived the second-order coefficient[39] to be

$$\frac{h(f)}{h_s} = 1 + \frac{5}{2}f + 6.2f^2, \tag{10}$$

which corresponds to $k_H = 0.992$.

For salt solutions, the viscosity is most commonly described by the Jones-Dole equation,[38] which is

$$\frac{h(c)}{h_s} = 1 + A\sqrt{c} + Bc. \tag{11}$$

This can be extended to higher concentrations as

$$\frac{h(c)}{h_s} = 1 + A\sqrt{c} + Bc + Dc^2, \tag{12}$$

where A, B, D are fit coefficients and $A\sqrt{c}$ represents the interactions and mobility of ions, which can be calculated using the Falkenhagen theory.[48,49] Here the term Bc represents ion-solvent interactions, and Dc^2 represents ion-dipole interactions and long-range coulombic ion-ion interactions.

Note that according to these models, as the concentration of solute increases, the viscosity of the solution increases, first linearly, then much more dramatically. The high viscosity can result in high pumping cost and reduced conductivity, and therefore lower the efficiency of RFBs. For our purposes, we use the term "flowable" to mean that the fluid viscosity is sufficiently low to be within the range of viscosity of known RFB working fluids. For example, viscosities up to 1 $\mathrm{Pa \times s}$ have been used in working RFBs.[50] Although there is no strict upper limit to the maximum possible viscosity in a RFB, since system-level architecture could possibly be changed to accommodate

higher viscosities, for practical purposes we treat as "flowable" any RFB solution that has viscosity lower than $1\ \mathrm{Pa \times s}$.

In this study, the Einstein, Huggins, and extended Jones-Dole equations were used to describe the measured viscosities. Molecular information, such as intrinsic viscosity, hydrodynamic diameter, Huggins coefficient, and the presence of ion interactions were determined from fit parameters. For comparing the hydrodynamic diameters, the representative geometries were optimized using Density Functional Theory (DFT), details in the SI. As the parameters are highly sensitive to small uncertainties in measurement, great attention was paid to the fit procedure and the most credible fit was determined from the Bayesian Information Criterion (BIC), which is introduced in the next section.

D. Fit method and credibility

The fit and model selection were done using the "fitnlm" function in MATLAB,[51] a commonly employed nonlinear regression model that uses an iterative generalized least squares algorithm, which in its most generalized form minimizes the residual sum of squares (RSS).[52] The weighting function was specified as the experimental uncertainty (standard deviation) of each measured data point, which propagates the uncertainty in measurement to the fit. That is,

$$\mathrm{RSS} = \sum_{i=1}^{n} \frac{\left(y_i - f\left(x_i\right)\right)^2}{u_i} \tag{13}$$

is minimized to determine the fit parameters. The data distribution and data density are important but subtle challenges to any data fit for the purpose of inference. In our case, we have higher data density at lower concentrations. Fitting to this uneven data distribution may emphasize the low concentration measurements, but we note that this is also the region most applicable to the theories described in Section 2.C.

To evaluate the hydrodynamic diameter and quantify the interaction of molecules in solution, the intrinsic viscosity and Huggins coefficient can be fit to the measured viscosities at given concentrations. However, the intrinsic viscosity is defined in the limit of $c \to 0$,[53] while all the measurements are done at finite concentrations. This is a known issue and various approaches have been used to resolve this conflict, such as single point method and extrapolation.[54] Here, the extrapolation method was employed by rearranging the Huggins equation as

$$\eta_{\mathrm{red}} = \frac{\eta/\eta_s - 1}{c} = \left[\eta\right] + k_H \left[\eta\right]^2 c, \tag{14}$$

where η_{red} is called the reduced viscosity. The reduced viscosity versus concentration is fit to a linear function and the intrinsic viscosity is evaluated as the intercept at zero concentration. Since the viscosity contributed by the solvent must be subtracted before extrapolation, small experimental errors can be amplified,[55] and this is addressed by including a weighting function in the fitting based on propagated uncertainty of the data, so that the uncertainty in concentration is accounted for in the reduced viscosity, which is used in model fit and selection. The most credible fit is found by comparing the Bayesian Information Criterion (BIC) for each fit result.

BIC is a criterion for model selection, which takes both the goodness of fit and the penalty term for the number of parameters in the model into account. It is an approximation of the full Bayes factors used to assess model credibility. While the full Bayesian calculation has been applied previously to complex fluid rheology,[56] the BIC approximation is much less computationally involved. It is calculated as

$$\mathrm{BIC} = -2\ln L + k\ln n, \tag{15}$$

where $\ln L$ is the log-likelihood, which represents the goodness of the fit, n is the number of data points used for fit, and k is the number of parameters in the model. For linear regression, the log-likelihood function can be written in terms of the RSS as[57]

$$\ln L = -\frac{n}{2}\left[\ln 2p + \ln\frac{\mathrm{RSS}}{n} + 1\right]. \tag{16}$$

The BIC is then calculated by

$$\mathrm{BIC} = -2\ln L + k\ln n = n\left[\ln 2p + \ln\frac{\mathrm{RSS}}{n} + 1\right] + k\ln n. \tag{17}$$

The second term on the right side is the penalty term acounting for over-parameterizing. Lower BIC corresponds to better credibility. The BIC increases in magnitude with n, which only improves the credibilty for sufficiently negative values of the square-bracket term, i.e. for sufficiently small RSS/n.

The viscosities of solutions of MEEPT and its cations were measured and analyzed using the methods mentioned above, and the results are discussed next.

3. RESULTS AND DISCUSSION

A. MEEPT: a flowable ROM

A wide range of concentrations of MEEPT/ACN solutions and neat MEEPT were studied. Neat MEEPT is a yellow, oily liquid, as shown in the photograph inset in Figure 2(a). It is miscible with ACN in any proportion. The viscosities of neat MEEPT and MEEPT/ACN solutions were measured over a wide range of shear rates, and Newtonian viscosities were observed for all samples within 5% variation, as shown in Figure 2(a). The error bars come from the standard deviation for repeat measurements.

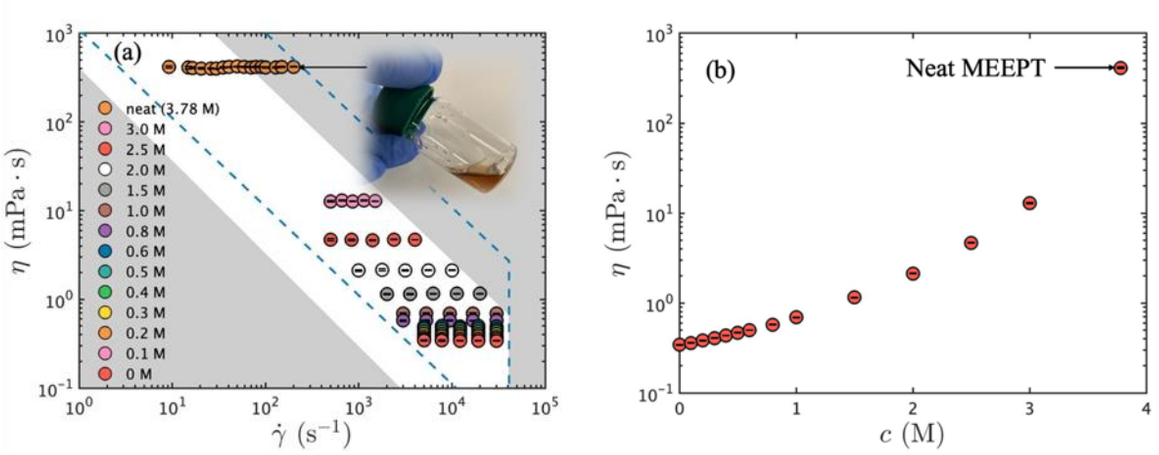

Figure 2. Viscosities of neat MEEPT and MEEPT/ACN solutions at different concentrations (0 – 3 M): (a) the dynamic viscosities as a function of shear rate $\dot{\gamma}$; the gray areas are the experimental limits for the measuring chip used for MEEPT/ACN solutions, and the blue dashed lines are the limits for the chip used for neat MEEPT, which are due to the maximum and minimum pressure drops that the pressure sensors can measure in the flow channel, (b) the average Newtonian viscosity as a function of MEEPT concentration. Note: the concentration of neat MEEPT is around 3.8 M.

The average Newtonian viscosity at each concentration was calculated by taking an average over viscosities at different shear rates; the error bars come from both the standard deviation and the uncertainty propagation, as shown in Figure 2(b). The viscosity of neat MEEPT is 412 mPa×s, 1,000 times larger than that of ACN. Therefore, as the MEEPT concentration increases, the viscosity of MEEPT/ACN solutions increases, first linearly in the dilute regime, then more dramatically when the concentration becomes larger than 1 M. Note that the viscosity is plotted on a log scale, and it increases over three orders of magnitude. The trend follows a viscosity mixing law with a single coupling term,[58] as detailed in Supporting Information (SI).

B. Viscosity of two supporting salts electrolytes

In RFB electrolytes, supporting salts are added to raise ionic conductivity and to provide counterions for charged ROMs. In this paper, the viscosities of two different supporting salt electrolytes, $TEABF_4$/ACN and LiTFSI/ACN were measured at different concentrations at shear rates of 5,000 to 35,000 s^{-1}, as shown in Figure 3. Both the $TEABF_4$/ACN and LiTFSI/ACN solutions show Newtonian behavior, within 5% variation.

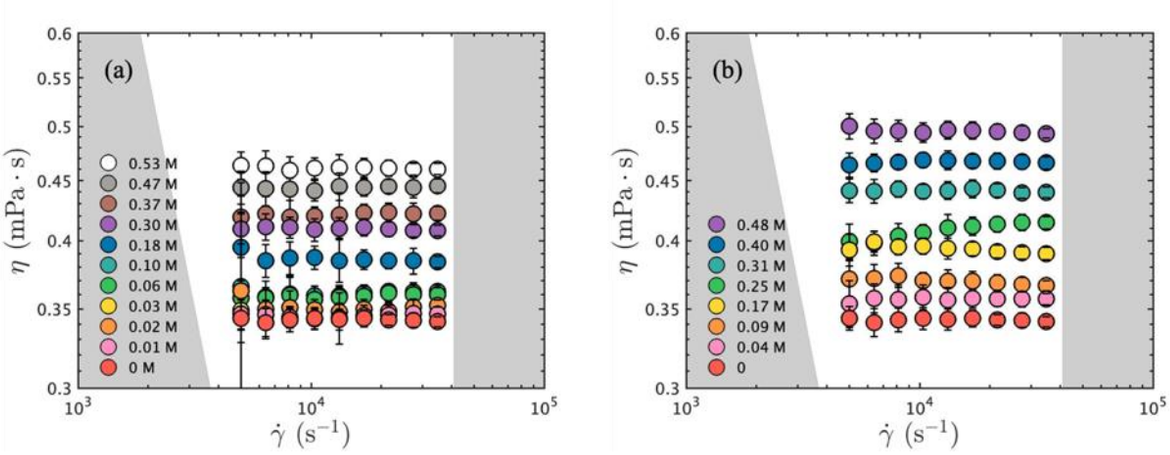

Figure 3. The dynamic viscosity of (a) $TEABF_4$ in ACN and (b) LiTFSI in ACN at 0 – 0.5 M as a function of shear rate. The viscosities show Newtonian behavior within 5% variation.

The average Newtonian viscosities for both supporting salts were obtained by taking an average of viscosities, with the error bars coming from standard deviation and uncertainty propagation, as shown in Figure 4(a). The viscosity of the salts in ACN solutions increases faster for LiTFSI than for $TEABF_4$. From Figure 4(b), it can be seen that unlike MEEPT, the reduced viscosities of $TEABF_4$ and LiTFSI decrease at first, then increase linearly, possibly suggesting that the hydrodynamic diameters decrease at first, which warrants including a square root term in the viscosity model. In the Jones-Dole equation, the $A\sqrt{c}$ term represents the interaction and mobility of ions and this term becomes less influential as concentration increases. Therefore, for salt solutions, the Jones-Dole and the extended Jones-Dole equations are fitted, where the BICs of the extended Jones-Dole equation fits are found to be lower for both salts (details in the SI). The solid lines in Figure 4 are the Jones-Dole equation fits and the dashed lines in Figure 4(b) are the extended Jones-Dole equation fit without the $A\sqrt{c}$ term. It can be seen that the two lines differ in the low concentration regime, then converge as the concentration increases. The *B* coefficient is interpreted as an intrinsic viscosity, and the hydrodynamic diameters and the Huggins coefficients are evaluated from the *B* and *D* coefficients respectively, as shown in Table 2. The hydrodynamic diameters of $TEABF_4$ and LiTFSI are calculated to be 8.06 ± 0.77 and 9.48 ± 0.73 Å respectively.

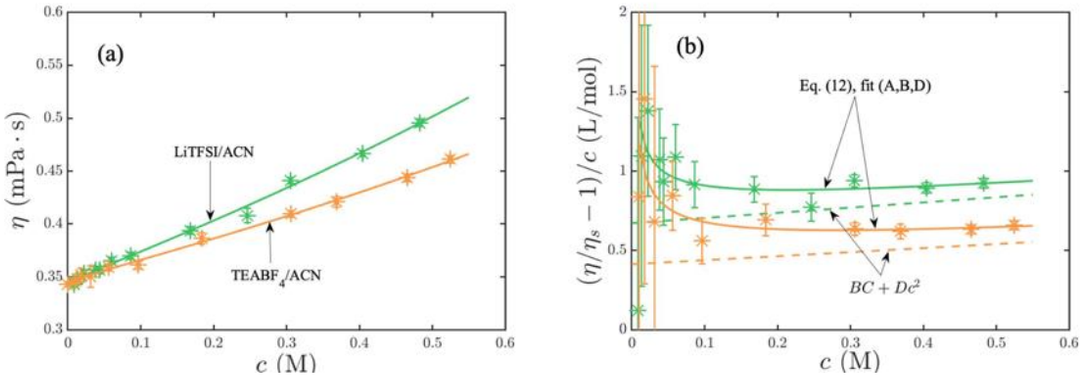

Figure 4. The viscometric analysis results of $TEABF_4$/ACN (orange) and LiTFSI/ACN (green) solutions as a function of salt concentration; (a) the average Newtonian viscosities, (b) the reduced viscosities; the solid lines show the extended Jones-Dole equation (Eq.12) fits, and the dashed lines are the fits without $A\sqrt{c}$ term, where the intercept is $[h]$, and the slope is proportional to k_H.

Table 2. $TEABF_4$ and LiTFSI, the most credible fit results of concentration-dependent average Newtonian viscosity to the extended Jones-Dole equation (Eq.12).

	c_{max} (M)	A ($L^{1/2}/mol^{1/2}$)	B (L/mol)	D (L^2/mol^2)	d_H (Å)	k_H (-)
$TEABF_4$	0.52	0.08 ± 0.04	0.41 ± 0.12	0.25 ± 0.14	8.06 ± 0.77	1.49 ± 0.94
LiTFSI	0.48	0.06 ± 0.05	0.67 ± 0.15	0.33 ± 0.22	9.48 ± 0.73	0.72 ± 0.52

To study the viscosities of MEEPT and charged MEEPT cations in different supporting salt environments, the ROMs are dissolved in electrolytes containing 0.5 M supporting salts. The viscosity of the electrolytes of 0.5 M $TEABF_4$ is the measured viscosity of $TEABF_4$ in ACN; the same holds for 0.5 M LiTFSI. At a concentration of 0.5 M, the viscosity of $TEABF_4$/ACN solution is 0.45 mPa·s, while the LiTFSI/ACN solution is 0.50 mPa·s.

C. MEEPT in different supporting salt environments

For MEEPT in ACN electrolytes containing supporting salts, the conformation and interactions between MEEPT molecules might change, which affects the viscosities of MEEPT solutions. Thus, viscosities of MEEPT in different supporting salt environments are studied. The measurement results, which show Newtonian behavior within 3% variation, are shown in the Figure 5.

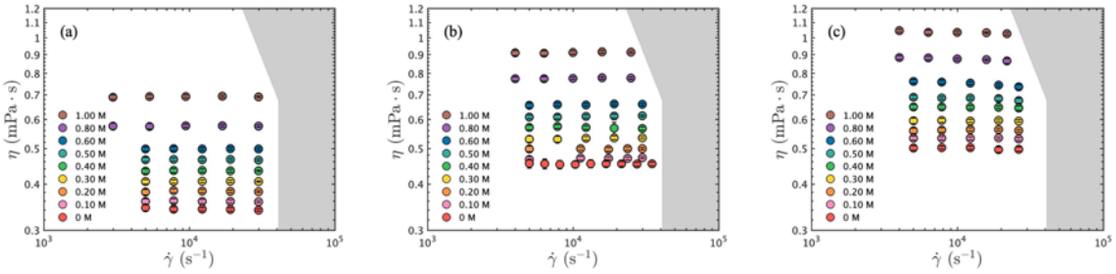

Figure 5. The dynamic viscosities of MEEPT/ACN solutions in different supporting salt environments, (a) no salt, (b) $TEABF_4$ (0.5 M), (c) LiTFSI (0.5 M); the viscosities show Newtonian behavior within 3% variation.

Similarly, the concentration-dependent average Newtonian viscosities for both solutions were calculated and plotted in comparison with the MEEPT/ACN solution, as shown in Figure 6(a). At zero MEEPT concentration, the viscosities of the three electrolytes are different, with 0.5 M LiTFSI/ACN > 0.5 M $TEABF_4$/ACN > ACN without supporting salt, but the increasing slopes are similar. To quantify the effect of supporting salts on the increase of viscosity versus MEEPT concentration, the reduced viscosity is plotted as a function of concentration (0.1 – 1.0 M), as shown by the data points in Figure 6(b), and is fit with the rearranged Huggins equation (Eq. (14)).

In the Huggins equation (Eq. (9)), only two factors are taken into account, namely the excluded volume described by the linear term, $[\eta]c$, and the interactions between particles, represented by the quadratic term, $k_H([\eta]c)^2$. If higher order terms can be neglected, the reduced viscosity, η_{red}, as shown in the rearranged Huggins equation (Eq. (14)), is a linear function of *c*. First, to determine the critical concentration at which the higher order terms become important and the Huggins equation no longer holds, the most credible fit in terms of concentration range for the Huggins equation was found. This was done by fitting the reduced viscosity versus concentration data to the rearranged Huggins equation (Eq. (14)) with different numbers of data points. By changing the maximum concentration used to fit, that is, 3 points from 0.1 to 0.3 M were fit to the equation, then 4 points from 0.1 to 0.4 M, and so on, until the maximum concentration tested was used. The BIC of each fit were compared, and the one with the minimum BIC is the most credible fit. The corresponding concentration range is the most appropriate range for the Huggins equation, beyond which the equation is no longer suitable. The fit results at each sample size are shown in the SI, and the fit lines over different concentration ranges are plotted in Figure 7. From fit results for MEEPT/ACN with no salt (red), the deviation of fit when using data at sufficiently high concentrations can be seen, as at such high concentrations, the viscosity increase is more dramatic and the Huggins equation no longer holds. From fit for MEEPT/ACN solutions with 0.5 M $TEABF_4$ (orange) and with 0.5 M LiTFSI (green), the fit lines using fewer data points at low concentration are oberserved to deviate from the data, due to the large uncertainty of the measurements in low concentration regime. The BIC of each fit is plotted versus the number of data points used for fit. It can be seen that for MEEPT/ACN with no salt (red), the BIC decreases with the number of data points, reaching its minimum at $n = 7$. This corresponds to concentrations ranging from 0.1 to 0.8 M, and the BIC then increases as *n* becomes larger. This means that until 0.8 M, the higher order term in the Huggins equation can be neglected and it is appropriate to use

it to describe the concentration-dependent viscosity. For solutions with 0.5 M $TEABF_4$ (orange) and with 0.5 M LiTFSI (green), the BIC decrerases with n, reaching its minimum at $n = 8$, which corresponds to a maximum concentration of 1.0 M. For solutions with 0.5 M LiTFSI, the minimum BIC at 3 data points was neglected as it gives unreasonable fit parameters, which comes from the large fluctuation at small concentrations. The most credible fit results are shown as solid lines in Figure 6, where in the reduced viscosity plot, the intercept represents $[\eta]$, and k_H is determined from the slope. Therefore, d_H of MEEPT can be determined from $[\eta]$ using Eq. (8), which are 8.52 ± 0.07, 7.72 ± 0.12, and 8.56 ± 0.16 Å for MEEPT/ACN solutions without supporting salts, with 0.5 M $TEABF_4$, and with 0.5 M LiTFSI, respectively. Table 3 summarizes these results.

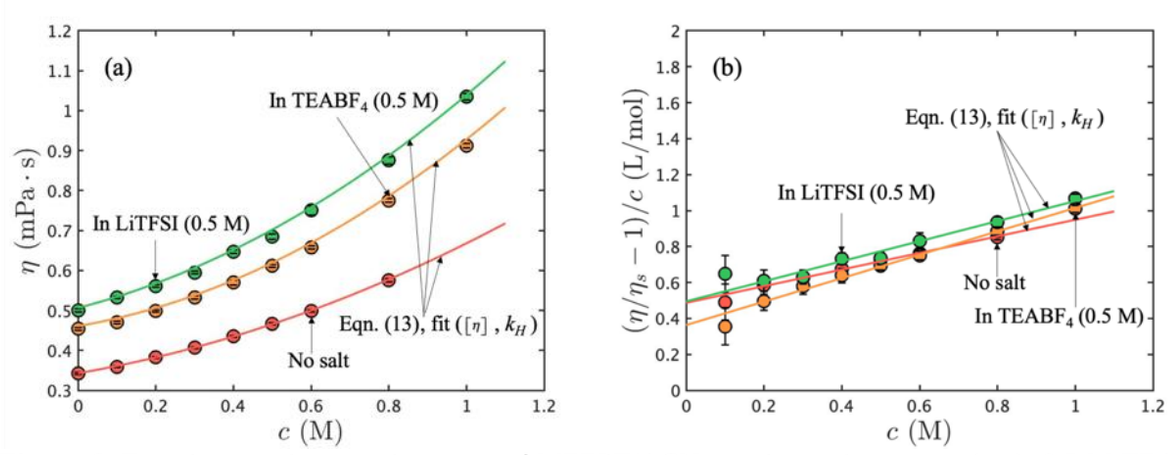

Figure 6. The viscometric analysis results of MEEPT/ACN solutions with no salt (red), 0.5 M $TEABF_4$ (orange), and 0.5 M LiTFSI (green) as a function of MEEPT concentration. The solid lines show the rearranged Huggins equation (Eq. (14)) fit; (a) the average Newtonian viscosities, (b) the reduced viscosities; intercept is $[\eta]$, and slope is proportional to k_H.

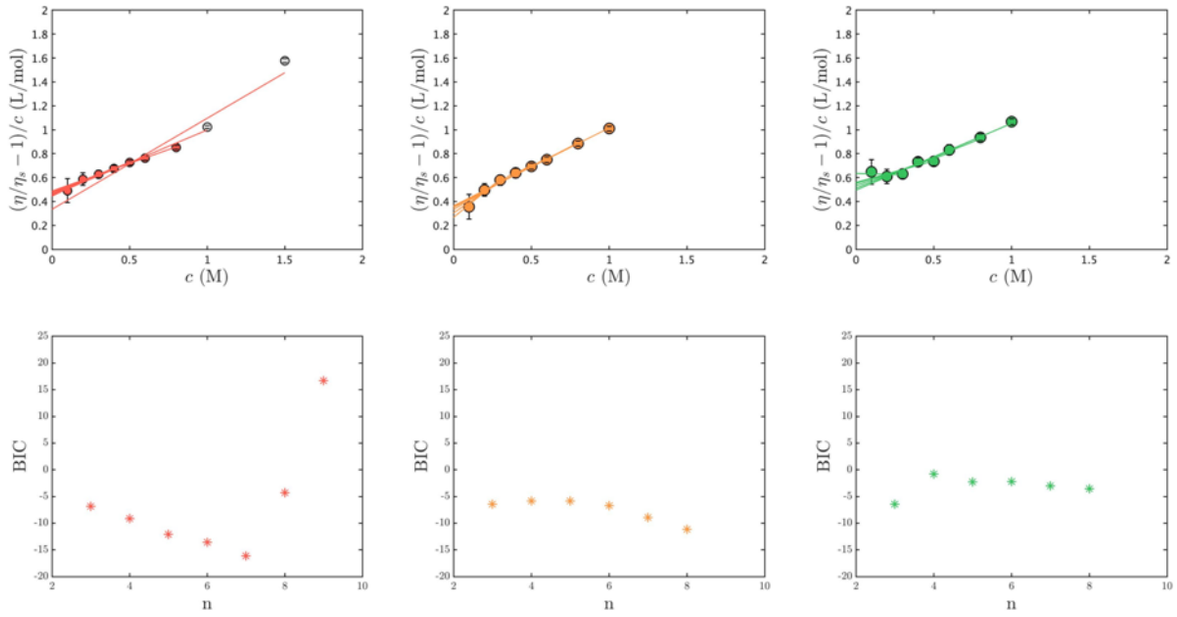

Figure 7. Fit procedure and selection of MEEPT/ACN solutions with no salt (red), 0.5 M $TEABF_4$ (orange) and 0.5 M LiTFSI (green): the reduced viscosities as a function of MEEPT concentrations, all the data are used to fit the rearranged Huggins equation (Eq. (13)), from which the hydrodynamic diameters and Huggins coefficients are determined. The credibility of fit: BIC as a function of *n*, fit to Eq. (14). For MEEPT/ACN solutions with no salt (red), $n = 7$ is the most credible fit according to the BIC, for solutions with 0.5 M $TEABF_4$ (orange) and with 0.5 M LiTFSI (green), $n = 8$ are the most credible fits.

Table 3. MEEPT in different supporting salt environments: the most credible fit results of concentration-dependent reduced viscosity to the rearranged Huggins equation (Eq. (14)).

	c_{max} (M)	h_s (mPa×s)	$[h]$ (L/mol)	d_H (Å)	k_H (-)
No salt	0.80	0.34 ± 0.01	0.49 ± 0.01	8.52 ± 0.07	1.95 ± 0.10
$TEABF_4$ (0.5 M)	1.00	0.46 ± 0.01	0.36 ± 0.02	7.72 ± 0.12	4.94 ± 0.29
LiTFSI (0.5 M)	1.00	0.50 ± 0.01	0.49 ± 0.03	8.56 ± 0.16	2.28 ± 0.21

The optimized structures of the neutral MEEPT molecule and their relative energies are shown in Figure 8, calculated using Density Functional Theory (DFT). The energy differences of the four optimized MEEPT molecules are within 0.2 eV. The dimensions of MEEPT molecules are specified. The molecular structure dimensions, which are about 7 to 11 Å, are comparable to the hydrodynamic diameters determined from viscosity measurements, and are almost equal within the experimental error in different supporting salts. This means that the addition of supporting salts does not have a significant effect on the hydrodynamic diameter of MEEPT.

The Huggins coefficients, which quantify the molecular interactions, are 1.95 ± 0.10, 4.94 ± 0.29, and 2.28 ± 0.21, respectively, calculated from the most credible fits to the rearranged Huggins equation. Compared with 0.992, which is the Huggins coefficient derived by Batchelor for

Browian hard spheres with only hydrodynamic inteactions and steric effects, those for MEEPT in different supporting salts are larger. This suggests that there are extra interactions between MEEPT molecules that contribute to the viscous dissipation at finite concentrations.

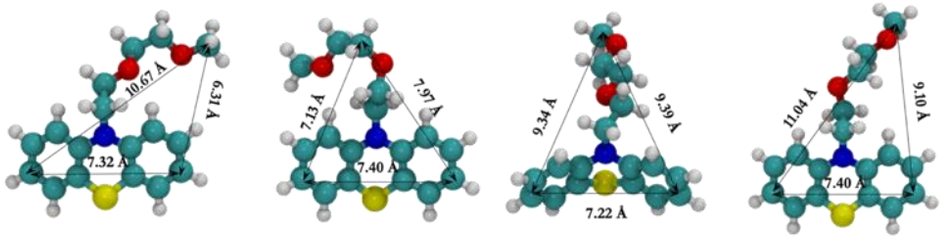

Figure 8. Four optimized geometries and relative dimensions of neutral MEEPT calculated from DFT. Blue, yellow, cyan, red, and white spheres denote the nitrogen, sulfur, carbon, oxygen, and hydrogen atoms, respectively. The relative energies of the four geometries from left to right are 0, 0.04, 0.05, and 0.16 eV, respectively.

MEEPT solutions containing different supporting salts represent the uncharged state of RFBs; when charged, solution viscosities are unknown because the excluded volume of anion and the effects of solubility limits of its charged form have not been quantified so far. The impact of supporting salts on the viscosities of the MEEPT radical cation salt solutions is also unknown. The viscous flow properties of MEEPT radical cation salt solutions are addressed next.

D. Charged MEEPT cations

The two radical cation salts of MEEPT are investigated here: MEEPT-BF_4 and MEEPT-TFSI. The solubilities of the species are around 0.5 M and 1 M, respectively, varying within 60% in different supporting salt environments, as shown in
Table **1**. MEEPT-TFSI is more soluble than MEEPT-BF_4 in all three conditions. For each radical cation, the addition of supporting salt changes the solubility, and different supporting salts have different effects; $TEABF_4$ reduces solubility more dramatically.

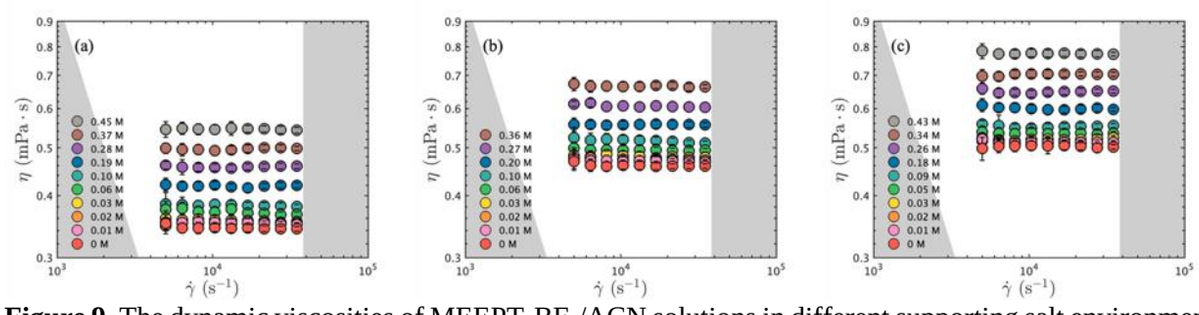

Figure 9. The dynamic viscosities of MEEPT-BF_4/ACN solutions in different supporting salt environments, (a) no salt, (b) $TEABF_4$ (0.5 M), and (c) LiTFSI (0.5 M); the solutions exhibit Newtonian behavior within 3% variation.

Results from viscosity measurements for MEEPT-BF_4 in three different environments (ACN, 0.5 M $TEABF_4$/ACN, and 0.5 M LiTFSI/ACN) are shown in Figure 9. The solutions are Newtonian within 3% variation. The average Newtonian viscosities at different concentrations were calculated

and plotted in Figure 10, with the error bars coming from standard deviation and uncertainty propagation. The slopes of MEEPT-BF_4 viscosities are almost the same for all three solutions.

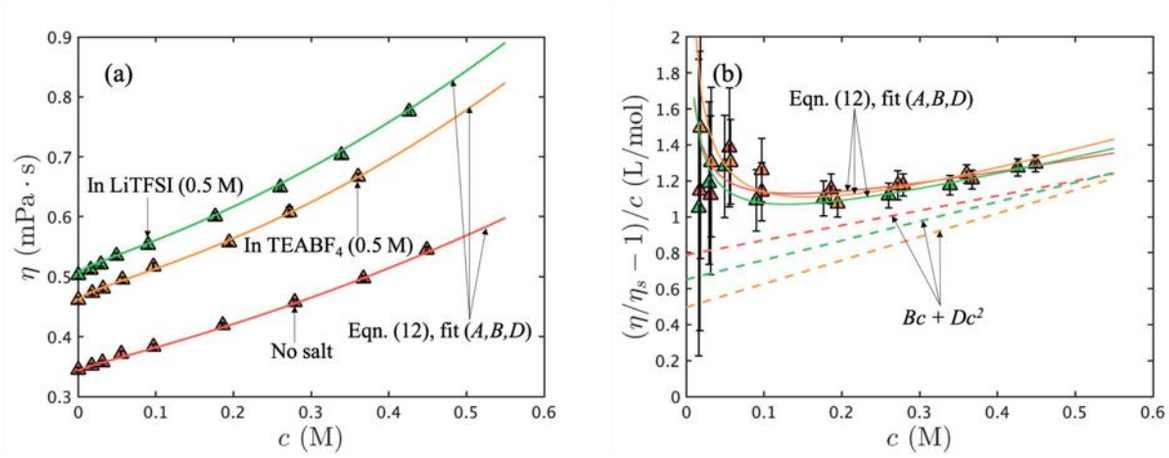

Figure 10. The viscometric analysis of MEEPT-BF_4/ACN solutions with no salt (red), 0.5 M $TEABF_4$ (orange), and 0.5 M LiTFSI (green) as a function of MEEPT-BF_4 concentration: (a) the average Newtonian viscosity, (b) the reduced viscosity; the solid lines are fits to the extended Jones-Dole equation, and the dashed lines are the fits without $A\sqrt{c}$ term, where the intercept is $[\eta]$, and the slope is proportional to k_H.

For charged cation solutions, the measured viscosities are fit to the Einstein (Eq. (5)), Huggins (Eq. (9)), Jones-Dole (Eq. (11)), and extended Jones-Dole equations (Eq. (12)). The details are shown in the SI. The extended Jones-Dole equation fits have the lowest BIC for all three solutions, and the results are shown as solid lines in Figure 10.

Table 4. MEEPT-BF_4 in different supporting salt environments, the most credible fit results of concentration-dependent average Newtonian viscosity to the extended Jones-Dole equation (Eq.(12)).

	c_{max} (M)	A ($L^{1/2}/mol^{1/2}$)	B (L/mol)	D (L^2/mol^2)	d_H (Å)	k_H (-)
No salt	0.45	0.08 ± 0.04	0.79 ± 0.14	0.82 ± 0.20	10.00 ± 0.59	1.33 ± 0.40
LiTFSI (0.5 M)	0.42	0.10 ± 0.03	0.65 ± 0.10	1.08 ± 0.17	9.38 ± 0.52	2.54 ± 0.57
$TEABF_4$ (0.5 M)	0.36	0.16 ± 0.05	0.50 ± 0.20	1.30 ± 0.36	8.58 ± 1.15	5.27 ± 2.56

From Figure 10(b), it can be seen that unlike MEEPT, the reduced viscosities of MEEPT-BF_4 decrease at first, then increase linearly, similar to that of supporting salts. This also suggests that the extended Jones-Dole equation should be used for fit. The dashed lines in Figure 10(b) are the extended Jones-Dole equation fits without the $A\sqrt{c}$ term. Thus the hydrodynamic diameter and the Huggins coefficient of MEEPT-BF_4 are calculated from the *B* and *D* coefficients, as shown in Table 4. The hydrodynamic diameters of MEEPT-BF_4 are 10.00 ± 0.59, 9.38 ± 0.52, and 8.58 ± 1.15 Å, respectively in the three electrolytes, with Huggins coefficients of 1.33 ± 0.40, 2.54 ± 0.50, and 5.27 ± 2.56 respectively. Therefore, we can conclude that the addition of supporting salts decreases the hydrodynamic diameter of MEEPT-BF_4, while promoting the interactions between MEEPT-BF_4 species.

In addition to MEEPT-BF_4, we also analyzed MEEPT-TFSI, which is more soluble than MEEPT-BF_4, as shown in
Table **1**. The results of its viscosity measurements are shown in Figure 11 in the three same electrolyte environments. The viscosities of MEEPT-TFSI in different solutions show Newtonian behavior even at 1 M, within 4% variation. Therefore, average Newtonian viscosities were calculated and plotted for the concentration-dependence analysis.

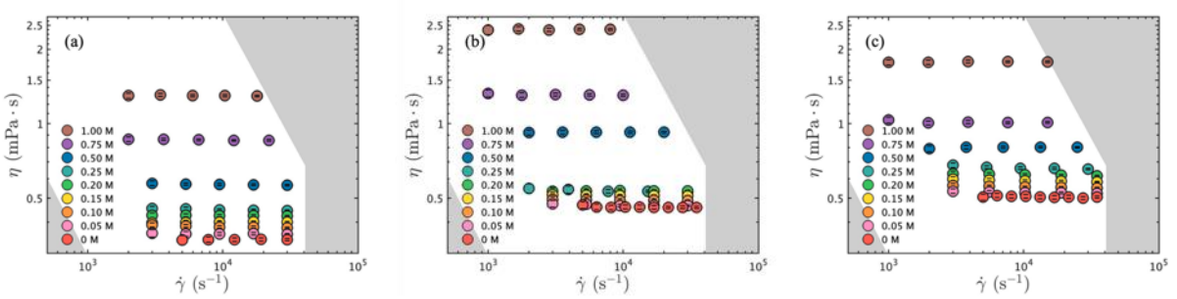

Figure 11. The dynamic viscosities of MEEPT-TFSI/ACN solutions in different supporting salt environments: (a) no salt, (b) $TEABF_4$ (0.5 M), and (c) LiTFSI (0.5 M); the solutions exhibit Newtonian behavior within 4% variation.

Figure 12 shows the average Newtonian viscosities and reduced viscosities of MEEPT-TFSI in the three electrolytes. Similar to MEEPT-BF_4, at concentrations up to 0.5 M, the viscosities of radical cation solutions increase slowly. However, as the concentration further increases, the higher order effects become significant and the viscosities increase dramatically, as MEEPT-TFSI approaches its maximum solubility limits.

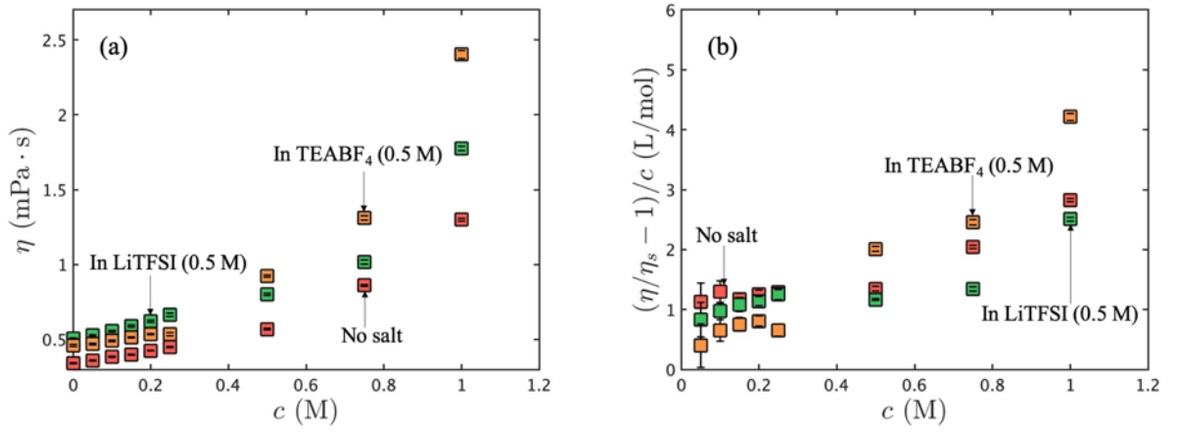

Figure 12. The viscosities of MEEPT-TFSI/ACN solutions with no salt (red), with 0.5 M $TEABF_4$ (orange), and with 0.5 M LiTFSI (green), as a function of MEEPT-TFSI concentration: (a) the average Newtonian viscosities, (b) the reduced viscosities.

From Figure 12(b), we can see that the reduced viscosities show increasing trend in the low concentration regime, which suggests an increasing apparent hydrodynamic diameter and a negative *A* coefficient in the Jones-Dole equation, which contradicts Falkenhagen theory.[48,49]

Currently, we are unable to describe such concentration-dependent viscosities using any equation available. Therefore, the apparent hydrodynamic diameters, $d_{\mathrm{app}} = \left(\frac{12B}{5\rho N_A} \right)^{1/3}$, were evaluated at a single concentration of 0.2 M, where the $A\sqrt{c}$ terms become insignificant and the reduced viscosities begin to increase linearly with concentration. The results are shown in Table 5.

Table 5. MEEPT-TFSI in different supporting environments: the apparent hydrodynamic diameters of MEEPT-TFSI at 0.20 M.

	d_{app}* (Å)
No salt	11.68 ± 0.22
$TEABF_4$ (0.5 M)	10.08 ± 0.37
LiTFSI (0.5 M)	11.31 ± 0.26

* d_{app} means the apparent hydrodynamic diameter at 0.2 M.

From the hydrodynamic diameter calculations, we see that the diameters for both MEEPT-BF_4 and MEEPT-TFSI increase compared to the neutral MEEPT and remain almost unchanged with the addition of supporting salts. The increase of hydrodynamic diameters is due to the excluded volume of anions, which can be seen in Figure 13. The DFT-optimized models show that the molecular structure dimensions of MEEPT-BF_4 and MEEPT-TFSI are a little larger compared with neutral MEEPT.

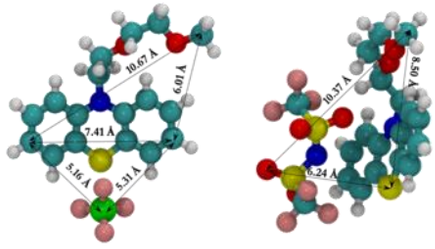

Figure 13. Optimized geometries of MEEPT-BF_4 and MEEPT-TFSI ion pair and their dimensions. Blue, yellow, cyan, red, white, pink, and green balls denote the nitrogen, sulfur, carbon, oxygen, hydrogen, fluorine, and boron atoms respectively.

When the concentration of MEEPT-TFSI becomes larger than 0.5 M. the viscosities of solutions increase dramatically, which means the interactions between MEEPT-TFSI molecules and between MEEPT-TFSI and supporting salts become more significant. In our work with other ROMs and supporting salt electrolytes, we have shown both experimentally and theoretically that the concentration of maximum ionic conductivity is associated with the concentration at which the viscosity begins to increase non-linearly,[59] which is about 0.5 M in this case. It can be seen from Figure 12(a) that the viscosity of MEEPT-TFSI in 0.5 M $TEABF_4$/ACN solution increases faster, and exceeds that of other solutions at 0.5 M, suggesting that the interactions in 0.5 M $TEABF_4$/ACN are stronger compared to those in others.

For MEEPT/ACN solutions (Figure 6), we observed that the viscosity increases linearly with concentration up to 0.5 M, no matter what supporting salts are used, and the increase is by less

than a factor of two, up to 1.0 M. However, for MEEPT-TFSI/ACN solutions (Figure 12), the viscosity increases dramatically at concentrations exceeding 0.5 M. This means that in the operation of NAqRFBs using MEEPT as the ROM, when MEEPT solutions are charged, the reconstitution of fluids at such high concentrations can greatly affect the viscous flow properties of the electrolyte, including viscosity, diffusion, and ionic conductivity.

Table 6 summarizes the results for all solutions tested.

Table 6. Summary of viscosity and hydrodynamic diameter results.

ROM	Electrolyte	Hydrodynamic diameter (Å)	Viscosity ($\mathrm{mPa \times s}$)	Concentration (M)	Analyzed by
MEEPT	ACN	8.52 ± 0.07	0.58 ± 0.01	0.80	Huggins equation
	0.5 M $TEABF_4$/ACN	7.72 ± 0.12	0.91 ± 0.01	1.00	
	0.5 M LiTFSI/ACN	8.56 ± 0.16	1.03 ± 0.01	1.00	
MEEPT-BF_4	ACN	10.00 ± 0.59	0.45 ± 0.01	0.45	Extended Jones-Dole equation
	0.5 M $TEABF_4$/ACN	9.38 ± 0.52	0.67 ± 0.01	0.42	
	0.5 M LiTFSI/ACN	8.58 ± 1.15	0.78 ± 0.01	0.36	
MEEPT-TFSI	ACN	11.68 ± 0.22	0.43 ± 0.01	0.20	Einstein equation one-point method
	0.5 M $TEABF_4$/ACN	11.31 ± 0.26	0.54 ± 0.01	0.20	
	0.5 M LiTFSI/ACN	10.08 ± 0.37	0.62 ± 0.01	0.20	

E. Discussion to rationalize Newtonian behavior

With the inference of hydrodynamic diameter in all the tested compositions, we can *a posteriori* rationalize the observation of Newtonian behavior up to shear rates of 30,000 s^{-1}. We do this by considering an estimate of a diffusion-based relaxation time[60,61] for a single MEEPT molecule,

$$\lambda = 6\pi\eta_s r_H^3 / (k_B T), \tag{18}$$

where $k_B T$ is the thermal energy, and postulating that non-Newtonian effects in steady shear become significant only when the Weissenberg number, defined as

$$\mathrm{Wi} = \lambda\dot{\gamma}, \tag{19}$$

becomes order unity. This number expresses the ratio between the rate at which the structure of the particle distribution is deformed by shear flow and the rate of Brownian diffusion that helps recover the equilibrium conformation. Weissenberg number is a general concept for fluid nonlinearity,[62] and here it relates specifically to the concept of a Péclet number, a ratio of advection rate to diffusion rate. We note that in the expression in Eq. (18), the time scale λ is a lower-bound estimate, since λ would increase sensitively with size (e.g. association of multiple molecules), increase linearly with background viscosity, and increase significantly at higher concentrations when intermolecular interactions become important.

For ACN solutions, for which $\eta_s = 0.34$ $\mathrm{mPa \times s}$, containing MEEPT with known hydrodynamic dimeter d_H = 8.5 Å, with negligible coulombic or van der Waals forces, flowing at a shear rate, $\dot{\gamma}$, ranging from 5,000 to 30,000 s^{-1}, and temperature, T = 298 K, the relaxation timescale, λ, is 0.12

ns, and the corresponding Weissenberg (Péclet) number ranges from 6×10^{-7} to 4×10^{-6}, much less than unity. From this, the solutions are expected to be Newtonian, as observed in our experiments. To show shear-thinning behavior, the Weissenberg (Péclet) number must be order unity or larger. We can define a critical shear rate for the condition Wi = 1, yielding for our specific case the critical shear rate

$$\dot{\gamma}_c = 8.4 \times 10^9 \text{ s}^{-1}, \tag{20}$$

which is much larger than the experimental limits. Thus, in our study, no shear-thinning is observed for any solution. Larger molecules, or aggregates of molecules, would change this estimate. For example, for a critical shear rate of 10,000 s^{-1} (within range of the instrument used here), the critical diameter is around 80 nm, which is about one hundred times larger than a single MEEPT molecule. From this analysis, the lack of shear-thinning implies that no structures of such size are contained within the complex fluid compositions tested here.

4. CONCLUSIONS

In summary, the viscous flow properties of MEEPT and its radical cation form were studied in different supporting salt environments, and it is shown that solution viscosity of both neutral and charged MEEPT increase as a result of excluded volume and species interactions; the excluded volume is comparable to the molecular size, while the interactions are greater than the hydrodynamic interactions. The hydrodynamic diameter of neutral MEEPT remains unchanged with the addition of supporting salts, while for charged MEEPT-BF_4, supporting salts decrease the hydrodynamic diameter and enhance interactions. For MEEPT-TFSI, which has a larger solubility compared with MEPPT-BF_4, the effects of interactions on the dramatical increase of viscosity at sufficiently high concentration was observed, and the apparent hydrodynamic diameters were calculated in this study, whose change is relative small with the addition of supporting salt. All the solutions are Newtonian, which is explained by comparing the time scale of shear rate to the diffusion-based relaxation time estimate.

It should be noted that the molecular information analysis is based on a continuum assumption, while the sizes of MEEPT and ACN are different by only one order of magnitude. Nonetheless, the hydrodynamic diameters determined from viscometric analysis are comparable to molecular structure dimensions, providing a reasonable estimate. The effect of supporting salts on bulk viscosity is studied, but more complex interactions and conformations of the molecule, such as ion association and liquid solvation, will be the subject of subsequent publications. Other transport properties, such as diffusivity and ionic conductivity versus concentration, remain to be studied, and will enable better prediction of the performance of MEEPT RFBs as well as gaining a better understanding of species association and solvation.

Importantly, the results presented here suggest that MEEPT is a promising ROM candidate with respect to transport properties, as it and its charged cation are “flowable” up to 0.5 M. The result also confirms that the MEEPT/ACN solutions behave like Newtonian liquids over a wide range of shear rates. For molecules with similar size, Newtonian behavior is expected as a result of the relaxation time scale. The model fit and selection method used here also provides a template to analyze measured solution viscosity, from which molecular information can be inferred.

SUPPORTING INFORMATION

The viscosity of LiTFSI and $TEABF_4$, the fit procedure of MEEPT and MEEPT-BF_4 are shown in supporting information.

ACKNOWLEDGMENTS

This work is supported by Joint Center for Energy Storage Research (JCESR), an Energy Innovation Hub funded by the U.S. Department of Energy.

DATA AVAILABILITY STATEMENT

The data that supports the findings of this study are available within the article [and its supplementary material].

REFERENCES

[1] A.Z. Weber, M.M. Mench, J.P. Meyers, P.N. Ross, J.T. Gostick, and Q. Liu, "Redox flow batteries: a review," J. Appl. Electrochem. **41**, 1137-1164 (2011).
[2] R.M. Darling, K.G. Gallagher, J.A. Kowalski, S. Ha, and F.R. Brushett, "Pathways to low-cost electrochemical energy storage: a comparison of aqueous and nonaqueous flow batteries," Energy Environ. Sci. **7**, 3459-3477 (2014).
[3] P. Leung, X. Li, C.P. de Leon, L. Berlouis, C.T. John Low, and F.C. Walsh, "Progress in redox flow batteries, remaining challenges and their applications in energy storage," RSC Adv. **2**, 10125-10156 (2012).
[4] M. Skyllas-Kazacos, M.H. Chakrabarti, S.A. Hajimolana, F.S. Mjalli, and M. Saleem, "Progress in flow battery research and development," J. Electrochem. Soc. **158**, R55-R79 (2011).
[5] G.L. Soloveichik, "Flow batteries: current status and trends," Chem. Rev. **115**, 11533 (2015).
[6] M.A. Goulet, L. Tong, D.A. Pollack, D.P. Tabor, S.A. Odom, A. Aspuru-Guzik, E.E. Kwan, R.G. Gordon, and M.J. Aziz, "Extending the lifetime of organic flow batteries via redox state management," J. Am. Chem. Soc. **141**, 8014-8019 (2019).
[7] J.A. Kowalski, L. Su, J.D. Milshtein, and F.R. Brushett, "Recent advances in molecular engineering of redox active organic molecules for nonaqueous flow batteries," Curr. Opin. Chem. Eng. **13**, 45-52 (2016).
[8] J. Zhang, R.E. Corman, J.K. Schuh, R.H. Ewoldt, I.A. Shkrob, and L. Zhang, "Solution properties and practical limits of concentrated electrolytes for nonaqueous redox flow batteries," J. Phys. Chem. C **122**, 8159-8172 (2018).
[9] K.L. Gering, "Prediction of electrolyte viscosity for aqueous and non-aqueous systems: Results from a molecular model based on ion solvation and a chemical physics framework," Electrochim. Acta **51**, 3125-3138 (2006).
[10] Z.P. Rosol, N.J. German, and S.M. Gross, "Solubility, ionic conductivity and viscosity of lithium salts in room temperature ionic liquids," Green Chem. **11**, 1453-1457 (2009).
[11] T. Katase, K. Murase, T. Hirato, and Y. Awakura, "Redox and transport behaviors of Cu(I) ions in TMHA-Tf2N ionic liquid solution," J. Appl. Electrochem. **37**, 339-344 (2007).
[12] J.L. Barton, J.D. Milshtein, J.J. Hinricher, and F.R. Brushett, "Quantifying the impact of viscosity on mass-transfer coefficients in redox flow batteries," J. Power Sources **399**, 133-143 (2018).
[13] V.A. Iyer, J.K. Schuh, E.C. Montoto, V.P. Nemani, S. Qian, G. Nagarjuna, J. Rodríguez-López,

R.H. Ewoldt, and K.C. Smith, "Assessing the impact of electrolyte conductivity and viscosity on the reactor cost and pressure drop of redox-active polymer flow batteries," J. Power Sources **361**, 334-344 (2017)

[14] H.W. Bindner, C. Krog Ekman, O. Gehrke, and F.R. Isleifsson, *Characterization of Vanadium Flow Battery* (Roskilde: Danmarks Tekniske Universitet, Risø Nationallaboratoriet for Bæredygtig Energi. Denmark., Denmark, 2010).

[15] L.J. Small, H.D. Pratt III, C.L. Staiger, and T.M. Anderson, "MetILs3: A strategy for high density energy storage using redox-active ionic liquids," Adv. Sustain. Syst. **1**, 1700066 (2017).

[16] Q. Xu, T.S. Zhao, L. Wei, C. Zhang, and X.L. Zhou, "Electrochemical characteristics and transport of Fe(II)/Fe(III) redox couple in a non-aqueous reline deep eutectic solvent," Electrochim. Acta **154**, 462-467 (2015).

[17] C. Zhang, T.S. Zhao, Q. Xu, L. An, and G. Zhao, "Effects of operating temperature on the performance of vanadium redox flow batteries," Appl. Energy **155**, 349-353 (2015).

[18] S. Kim, M. Vijayakumar, W. Wang, J. Zhang, B. Chen, Z. Nie, F. Chen, J. Hu, L. Li, and Z. Yang, "Chloride supporting electrolytes for all-vanadium redox flow batteries," Phys. Chem. Chem. Phys. **13**, 18186-18193 (2011).

[19] X. Li, J. Xiong, A. Tang, Y. Qin, J. Liu, and C. Yan, "Investigation of the use of electrolyte viscosity for online state-of-charge monitoring design in vanadium redox flow battery," Appl. Energy **211**, 1050-1059 (2018).

[20] N. Wang, Y. Chen, H. Han, M. Cao, X. Bi, S. Peng, and X. Cheng, "Influence of L-cystine as additive in the negative electrolyte on performance of vanadium redox flow battery," Int. J. Electrochem. Sci. **12**, 2893-2908 (2017).

[21] M. Burgess, K. Hernández-Burgos, J.K. Schuh, J. Davila, E.C. Montoto, R.H. Ewoldt, and J. Rodríguez-López, "Modulation of the electrochemical reactivity of solubilized redox active polymers via polyelectrolyte dynamics," J. Am. Chem. Soc. **140**, 2093-2104 (2018).

[22] M.T. Zafarani-Moattar and R. Majdan-Cegincara, "Viscosity modeling and prediction of aqueous mixed electrolyte solutions," Ind. Eng. Chem. Res. **48**, 5833-5844 (2009).

[23] X. Li, Y. Qin, W. Xu, J. Liu, J. Yang, Q. Xu, and C. Yan, "Investigation of electrolytes of the vanadium redox flow battery (IV): measurement and prediction of viscosity of aqueous VOSO4 solution at 283.15 K to 323.15 K, " J. Mol. Liq. **224**, 893-899 (2016).

[24] X. Li, C. Jiang, J. Liu, Y. Qin, Z. Zhang, Z. Liu, J. Yang, and C. Yan, "Prediction of viscosity for high-concentrated ternary solution (CH3SO3H+VOSO4+H2O) in vanadium flow battery, " J. Mol. Liq. **297**, 111908 (2020).

[25] X. Li, C. Jiang, Y. Qin, J. Liu, J. Yang, Q. Xu, and C. Yan, "Investigation of electrolytes of the vanadium redox flow battery (VII): Prediction of the viscosity of mixed electrolyte solution (VOSO4+H2SO4+H2O) based on Eyring's theory, " J. Chem. Thermodyn. **134**, 69-75 (2019).

[26] E.R. Logan, E.M. Tonita, K.L. Gering, and J.R. Dahn, "A critical evaluation of the advanced electrolyte model," J. Electrochem. Soc. **165**, A3350-A3359 (2018).

[27] C.W. Macosko, *RHEOLOGY: Principles, Measurements, and Applications* (VCH Publishers. Inc., New York, 1994).

[28] A. Ogawa, H. Yamada, S. Matsuda, K. Okajima, and M. Doi, "Viscosity equation for concentrated suspensions of charged colloidal particles," J. Rheol. **41**, 769-785 (1997).

[29] B.D. Todd and P.J. Daivis, "Homogeneous non-equilibrium molecular dynamics simulations of viscous flow: techniques and applications," Mol. Simul. **33**, 189-229 (2007).

[30] D.J. Evans and W.B. Streett, "Transport properties of homonuclear diatomics II. dense fluids," Mol. Phys. **36**, 161-176 (1978).

[31] D.J. Evans, "The frequency dependent shear viscosity of methane," Mol. Phys. **37**, 1745-1754 (1979).
[32] I. Borzsák, P.T. Cummings, and D.J. Evans, "Shear viscosity of a simple fluid over a wide range of strain rates," Mol. Phys. **100**, 2735-2738 (2002).
[33] J. Petravic, "Shear stress relaxation in liquids, " J. Chem. Phys. **120**, 10188-10193 (2004).
[34] Y. Zhang, L. Xue, F. Khabaz, R. Doerfler, E.L. Quitevis, R. Khare, and E.J. Maginn, "Molecular topology and local dynamics govern the viscosity of imidazolium-based ionic liquids," J. Phys. Chem. B **119**, 14934-14944 (2015).
[35] J.D. Milshtein, A.P. Kaur, M.D. Casselman, J.A. Kowalski, S. Modekrutti, P.L. Zhang, N.H. Attanayake, C.F. Elliott, S.R. Parkin, C. Risko, F.R. Brushett, and S.A. Odom, "High current density, long duration cycling of soluable organic active species for non-aqueous redox flow batteries," Energy Environ. Sci. **9**, 3531-3543 (2016).
[36] A. Einstein, *A New Determination of Molecular Dimensions*, PhD thesis, Unviersity of Zurich, 1905.
[37] M.L. Huggins, "The viscosity of dilute solutions of long-chain molecules. IV. dependence on concentration," J. Am. Chem. Soc. **64**, 2716-2718 (1942).
[38] G. Jones and M. Dole, "The viscosity of aqueous solutions of strong electrolytes with special reference to barium chloride," J. Am. Chem. Soc. **51**, 2950-2964 (1929).
[39] G.K. Batchelor, "The effect of Brownian motion on the bulk stress in a suspension of spherical particles," J. Fluid Mech. **83**, 97-117 (1977).
[40] A.P. Kaur, O.C. Harris, N.H. Attanayake, Z. Liang, S.R. Parkin, M.H. Tang, and S.A. Odom, "Quantifying environmental effects on the solution and solid-state stability of phenothiazine radical cations," Chem. Mater. in press (2020).
[41] C. Reichardt, "Solvatochromic dyes as solvent polarity indicators," Chem. Rev. **94**, 2319-2358 (1994).
[42] J. Maes, L. Verlooy, O.E. Buenafe, P.A.M. de Witte, C. V. Esguerra, and A.D. Crawford, "Evaluation of 14 organic solvents and carriers for screening allications in zebrafish embryos and larvae," PLoS One **7**, 1-9 (2012).
[43] R.H. Ewoldt, M.T. Johnston, and L.M. Caretta, *Experimental Challenges of Shear Rheology: How to Avoid Bad Data* (Springer, 2015).
[44] RhenSense Inc., m-VROC Viscometer-Controlled Shear Rates and Small Samples: Https://Www.Rheosense.Com/Products/Viscometers/m-Vroc/Overview.
[45] Ad Hoc Committee Official Nomenclature and Symbols, "Official symbols and nomenclature of The Society of Rheology," J. Rheol. **57**, 1047-1055 (2013).
[46] T. Jyothi Latha and S. Jayanti, "Hydrodynamic analysis of flow fields for redox flow battery applications," J. Appl. Electrochem. **44**, 995-1006 (2014).
[47] Y.K. Zeng, X.L. Zhou, L. Zeng, X.H. Yan, and T.S. Zhao, "Performance enhancement of iron-chromium redox flow batteries by employing interdigitated flow fields," J. Power Sources **327**, 258-264 (2016).
[48] H. Falkenhagen, "Viscosity of electrolytes," Nature **127**, 439-440 (1931).
[49] H. Falkenhagen and E.L. Vernon, "LXII. The viscosity of strong electrolyte solutions according to electrostatic theory," London, Edinburgh, Dublin Philos. Mag. J. Sci. **14**, 537-565 (1932).
[50] M. Duduta, B. Ho, V.C. Wood, P. Limthongkul, V.E. Brunini, W.C. Carter, and Y.-M. Chiang, "Semi-solid lithium rechargeable flow battery," Adv. Energy Matls. **1**, 511-516 (2011).
[51] Natick, *MATLAB. Version 7.10.0 (R2019a).* (Massachusetts: The MathWorks Inc., 2019).
[52] P.K. Singh, J.M. Soulages, and R.H. Ewoldt, "On fitting data for parameter estimates: residual

weighting and data representation," Rheol. Acta **58**, 341-459 (2019).
[53] P.C. Hiemenz and T.P. Lodge, *Polymer Chemistry*, 2nd Ed. (CPC Press, 2007).
[54] P.A. Lovell, "Dilute solution viscometry," Compr. Polym. Sci. Suppl. **1**, 173-197 (1989).
[55] R.G. Larson, *The Structure and Rheology of Complex Fluids* (Oxford University Press, Inc., New York, 1999).
[56] J.B. Freund and R.H. Ewoldt, "Quantitative rheological model selection: good fits versus credible models using Bayesian inference," J. Rheol. **59**, 667-701 (2015).
[57] D. Sivia and J. Skilling, *Data Analysis: A Bayesian Tutorial*, 2nd Ed. (Oxford University Press, 2006).
[58] L. Grunberg and A.H. Nissan, "Mixture law for viscosity," Nature **164**, 799-800 (1949).
[59] N.H. Attanayake, Z. Liang, Y. Wang, A.P. Kaur, G. Baggi, S.R. Parkin, J.K. Mobley, R.H. Ewoldt, J. Landon, and S.A. Odom, "Supporting-salt-free concentration nonaqueous redox flow cell electrolytes containing permanetly charged active materials," Unpublished Results.
[60] I.M. Krieger, "A dimensional approach to colloid rheology," Trans. Soc. Rheol. **7**, 101-109 (1963).
[61] J.C. van der Werff and C.G. de Kruif, "Hard-sphere colloidal dispersions: The scaling of rheological properties with particle size, volume fraction, and shear rate," J. Rheol. **33**, 421-454 (1989).
[62] J.M. Dealy, "Weissenberg and Deborah numbers - their definition and use," Rheol. Bull. **79**, 14-18 (2010).

Physics of Fluids

(a) Microfluidic m-VROC viscometer

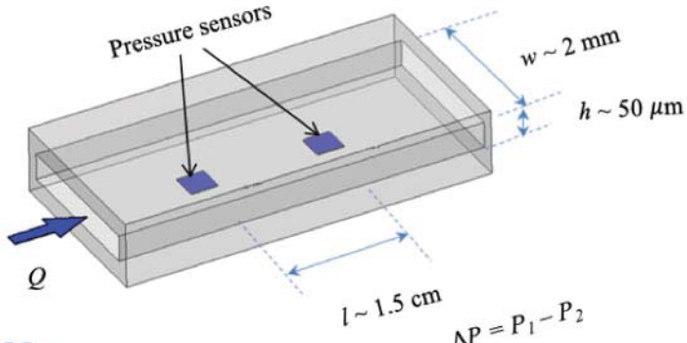

(b) ROMs

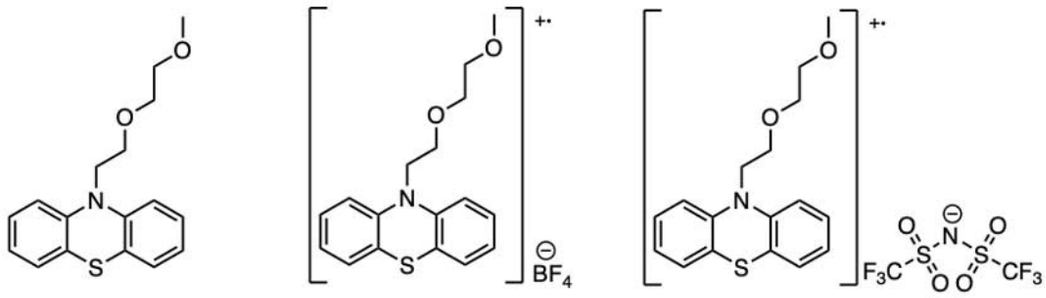

(c) Solvent

(d) Supporting salts